Modeling of Dyakonov surface waves at magnetized plasma–dielectric interface

BADER ALHASSON[1], MUHAMMAD UMAIR[2,*], FAWWAZ HAZZAZI[1], ABDUL GHAFFAR[2,*]
[1]*Department of Electrical Engineering, College of Engineering in Al-Kharj, Prince Sattam, Saudi Arabia*
[2]*Department of Physics, University of Agriculture, Faisalabad 38000, Pakistan*

This study examines the behavior of magnetically controlled Dyakonov surface waves at plasma-dielectric interface in THz frequency region. We analyze the influence of cyclotron and plasma frequencies on different properties of electromagnetic (EM) surface waves such as effective mode index, propagation loss, and normalized phase velocity. Our results show that as cyclotron frequency increases, the effective mode index increases, while the propagation loss decreases. However, increasing plasma frequency reduces effective mode index and increases propagation loss. Furthermore, higher wave frequency reduces the normalized phase velocity for both plasma features. Additionally, variations in plasma frequency and cyclotron frequency have a substantial impact on the normalized phase velocity. These findings may have promising applications in THz nanophotonic devices, plasmonic chips, sensors, near-field communication, and modulators.

(Received October 5, 2025; accepted June 2, 2026)

Keywords: Dyakonov Surface Waves, Magnetized plasma, Effective mode index, Propagation loss, Boundary conditions

1. Introduction

Electromagnetic (EM) surface waves are localized at the interfaces of two dissimilar mediums and exponentially decay as it propagates away from the interface [1-9]. There are different kinds of EM surface waves (SW), each associated with a specific type of interface. Zenneck examined the propagation of SW at radio frequencies, focusing on the planar interfaces between lossless and lossy dielectric materials. It was examined that metal-dielectric interfaces support the propagation of surface plasmon-polaritons (SPPs) waves [10]. The Tamm surface waves are supported by two isotropic dielectric materials. In contrast, Dyakonov surface waves (DSWs) produced between two dielectric materials among one of them should be anisotropic [11, 12]. Although partnering optical materials may be identical and anisotropic, they must be oriented in such a way that the eigenvectors of their permittivity dyadic are not aligned with each other. Based on the assumption that there is negligible energy loss in bulk optical materials on either side of the interface, DSWs could serve the same function as SPPs by transmitting energy at the interface, enable diverse applications in optics community.

DSWs is characterized by several distinctive features, one of the most notable being its narrow propagation range, usually spanning only few degrees [13, 14]. Moreover, DSWs display wide angular range when interacting with dissipative or magnetic materials, underscore their unique characteristics. The distinctive optical traits of DSWs such as tunability, non-reciprocal behavior, enhanced light-matter interaction, and surface sensing capabilities, position them as highly promising for groundbreaking applications in optics sector [1, 2]. Contrary to SPPs, which are purely transverse magnetic (TM) polarized, DSWs exhibit a hybrid nature, involving a combination of both transverse electric (TE) and TM polarization [3]. F. M. Marchevsky [4] and M. I. [5] Dyakonov developed the initial theoretical framework using anisotropic crystal interfaces. Experimental investigation of DSWs has shown significant potential as an important tool in optics community [6, 7]. It is becoming more prevalent to employ these waves in applications such as optical modulators, plasmonic sensors, and surface-enhanced spectroscopy, demonstrating their versatility and significance in the advancement of optical technology [3, 8, 9]. Uniaxial and biaxial optical materials are widely utilized in materials science to propagate DSWs. Theoretical researchers have employed different approaches to investigate DSWs' properties. M. V. Zakharchenko and G. F. Glinskii performed an analysis of DSWs propagation between two biaxial anisotropic mediums [10]. Juan J. Miret et. al. conducted study on the DSWs, exploring hybrid polarization techniques to broaden the angular range with minimal propagation losses. Sipeng Chen et al. studied the numerical modelling of DSWs between an isotropic medium and a conductor-backed uniaxial slab at planar structure [11]. Chenzhang Zhou et al. numerically analyzed the propagation of Dyakonov–Tamm (DT) SW at the planar structure between a nonhomogeneous uniaxial dielectric and an isotropic dielectric [12]. Osamu Takayama et al. experimentally analyzed the existence of DSWs anisotropic crystal [13]. Osamu Takayama et al. also reported the observation of Dyakonov plasmon supported at hyperbolic metamaterial [14]. Currently, the most interesting anisotropic materials are metamaterials due to their tailored properties rather than naturally occurring crystals [15, 16]. The unique and fascinating properties of plasma metamaterial have attracted significant attention in the field of optics [17-22]. Wave propagation in anisotropic media is significantly facilitated by plasma medium and offer innovative solutions to various challenges in the waveguide community [17-20]. Researchers classify plasma into two major categories: unmagnetized plasma and magnetized plasma. Unmagnetized plasma is characterized by the absence of an external magnetic field. In the presence of a magnetic field, plasma becomes magnetized, and its permittivity is described by its tensor [23]. The plasma frequency and cyclotron frequency can be used to control this permittivity. A lot of research have been conducted on unmagnetized plasma [24-30]. However magnetized plasma provides an additional degree of freedom compared to unmagnetized plasma due to presence of external magnetic field [31].

In this manuscript, we have analyzed magnetically control DSWs at magnetized plasma–dielectric interface. Behavior of DSWs is analyzed under different plasma features (plasma frequency, cyclotron frequency) in THz frequency region to analyze effective mode index, propagation loss and normalized phase velocity.

2. Theoretical formulations

Consider DSWs propagate along z-axis. Regions 1 and 2 describe the magnetized plasma and dielectric medium, respectively as shown in Fig. 1.

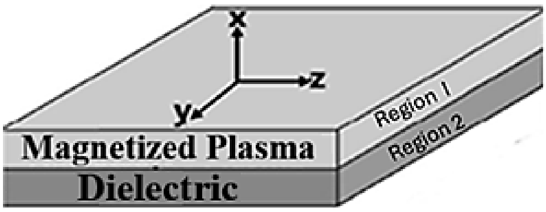

Fig. 1. Schematic view of DSWs at magnetized plasma–dielectric interface

The constitutive relations for magnetized plasma are:

$$\mathrm{D} = \varepsilon_0 \bar{\bar{\varepsilon}}.\mathrm{E} \tag{1}$$

$$\mathrm{H} = 1/\mu_0 \mathrm{B} \tag{2}$$

μ_0 and ε_0 are the permeability of free space and permittivity of free space, respectively, and $\bar{\bar{\varepsilon}}$ is the permittivity tensor for plasma medium.

$$[\bar{\bar{\varepsilon}}] = \begin{bmatrix} \varepsilon_1 & -j\varepsilon_2 & 0 \\ j\varepsilon_2 & \varepsilon_1 & 0 \\ 0 & 0 & \varepsilon_3 \end{bmatrix} \tag{3}$$

where ε_1, ε_2 and ε_3 are the permittivity tensor described in [32].

$$\varepsilon_1 = \varepsilon_0 (1 - \frac{(\omega_p)^2}{(\omega)^2 - (\omega_c)^2}) \tag{4}$$

$$\varepsilon_2 = \varepsilon_0 (1 - \frac{\omega_c * (\omega_p)^2}{\omega * ((\omega)^2 - (\omega_c)^2)}) \tag{5}$$

$$\varepsilon_3 = \varepsilon_0 (1 - \frac{(\omega_p)^2}{(\omega)^2}) \tag{6}$$

$$\omega_p = \sqrt{\frac{ne^2}{m\varepsilon_0}} \tag{7}$$

$$\omega_c = \frac{eB}{m} \tag{8}$$

ω, ω_p and ω_c represent the incident wave frequency, plasma frequency and cyclotron frequency, of magnetized plasma medium, respectively. While m, e, n and B denote the electron mass, electron charge, number density (electron density) and external magnetic field, respectively. The wave equation for H_z and E_z in the nonhomogeneous plasma can be written as follows:

$$\begin{bmatrix} \nabla^2 E_{z1} \\ \nabla^2 H_{z1} \end{bmatrix} + \begin{bmatrix} U_1 & jU_2 \\ jU_3 & U_4 \end{bmatrix} \begin{bmatrix} E_{z1} \\ H_{z1} \end{bmatrix} = 0 \tag{9}$$

where

$$\nabla = \hat{e}_x \frac{\partial}{\partial x} + \hat{e}_y \frac{\partial}{\partial y} + \hat{e}_z \frac{\partial}{\partial z} \tag{10}$$

$$U_1 = -(\frac{\beta^2 \varepsilon_3}{\varepsilon_1} - \omega^2 \mu_0 \varepsilon_3) \tag{11}$$

$$U_2 = \frac{\omega \mu_0 \beta \varepsilon_2}{\varepsilon_1} \tag{12}$$

$$U_3 = -\beta \omega \varepsilon_3 \frac{\varepsilon_3}{\varepsilon_1} \tag{13}$$

$$U_4 = \frac{\omega^2 \mu_0 \varepsilon_1^2 - \omega^2 \mu_0 \varepsilon_2^2)}{\varepsilon_1} - \beta^2 \tag{14}$$

The eigenvalues are:

$$s_1 = \sqrt{\frac{1}{2}(U_1 + U_4) + \frac{1}{2}\sqrt{(U_1 - U_4)^2 - 4U_2 U_3}} \tag{15}$$

$$s_2 = \sqrt{\frac{1}{2}(U_1 + U_4) + \frac{1}{2}\sqrt{(U_1 - U_4)^2 - 4U_2 U_3}} \tag{16}$$

EM fields for nonhomogeneous plasma are as follows:

$$E_{z1} = (A_1 e^{-q_1 x} + A_2 e^{-q_2 x}) e^{-j\beta z} \tag{17}$$

$$H_{z1} = j(A_1 \alpha_1 e^{-q_1 x} + A_2 \alpha_2 e^{-q_2 x})\, e^{-j\beta z} \tag{18}$$

β define the propagation constant. The rest of magnetized plasma fields component can be derived as [33].

$$E_t = ja\nabla_t E_z + b\nabla_t E_z \times a_z + c\nabla_t H_z + jd\nabla_t H_z \times a_z \tag{19}$$

$$H_t = e\nabla_t E_z + jf_1 \nabla_t E_z \times a_z + ja\nabla_t H_z + b\nabla_t H_z \times a_z \tag{20}$$

where a, b, c, d, e and f are given as:

$$a = \frac{U_3\omega\mu_0\varepsilon_2 - U_4\beta\varepsilon_3}{\varepsilon_1(U_1U_4 + U_2U_3)} \quad (21)$$

$$b = -\frac{U_3\omega\mu_0}{U_1U_4 + U_2U_3} \quad (22)$$

$$c = -\frac{U_1\omega\mu_0\varepsilon_2 + U_2\beta\varepsilon_1}{\varepsilon_1(U_1U_4 + U_2U_3)} \quad (23)$$

$$d = -\frac{U_1\omega\mu_0}{U_1U_4 + U_2U_3} \quad (24)$$

$$e = -\frac{U_3\beta*\varepsilon_1}{\varepsilon_1(U_1U_4 + U_2U_3)} \quad (25)$$

$$f_1 = \frac{U_4\omega\varepsilon_2}{(U_1U_4 + U_2U_3)} \quad (26)$$

$$q_1 = \sqrt{\beta^2 - {s_1}^2} \quad (27)$$

$$q_2 = \sqrt{\beta^2 - {s_2}^2} \quad (28)$$

$$\alpha_1 = \frac{U_1 - {q_1}^2}{U_2} \quad (29)$$

$$\alpha_2 = \frac{U_1 - {q_2}^2}{U_2} \quad (30)$$

In equations 29 and 30, α_1 and α_2 are hybrid mode factors. The fields phasor for free space is given below:

$$E_{y2} = A_3\, e^{\gamma x} e^{-j\beta z} \quad (31)$$

$$H_{y2} = A_4\, e^{\gamma x} e^{-j\beta z} \quad (32)$$

$$E_{z2} = A_4\left(\frac{j\gamma}{\omega\varepsilon_0}\right) e^{\gamma x} e^{-j\beta z} \quad (33)$$

$$H_{z2} = A_3\left(-\frac{j\gamma}{\omega\mu_0}\right) e^{\gamma x} e^{-j\beta z} \quad (34)$$

where,
$\gamma = \sqrt{\beta^2 - k_0^2}$ describe the wavenumber of free space.

Here A_1, A_2, A_3 and A_4 are amplitudes constant. Following boundary conditions are applied to obtain the characteristic equation.

$$\hat{x}\times(H_1 - H_2) = 0 \quad (35)$$

$$\hat{x}\times(E_1 - E_2) = 0 \quad (36)$$

$$\gamma q_2(-b\varepsilon_0\omega + \alpha_2(d\varepsilon_0\omega + (b^2 + df_1)\gamma q_1) - (\mu_0\omega(f_1 + b\alpha_2) + (b^2 + df_1)\gamma q_1)\alpha_1) + \omega(b\gamma\varepsilon_0 q_1 - \varepsilon_0(\mu_0\omega + d\gamma q_1)\alpha_1 + \mu_0\alpha_2(\varepsilon_0\omega + \gamma q_1(f_1 + b\alpha_1))) = 0 \quad (37)$$

3. Numerical results and discussion

In this section, numerical results of magnetically controlled DSWs at plasma dielectric interfaces are analyzed in THz frequency region by using dispersion relation (37). Here, we use collisionless plasma medium. Magnetized plasma provides an additional degree freedom due to the presence of magnetic field. Firstly, we analyze the effect of plasma and cyclotron frequencies on effective mode index and propagation loss. Since plasma frequency and cyclotron frequencies are the functions of number density and external magnetic field as reported in [40]. Effective mode index $Re\left(\frac{\beta}{k_0}\right)$ is very crucial parameter nanophotonic devices. Throughout calculations, we set numerical parameters: ω_p=10 THz, ω_c=$8 * 10^{13} Hz$ and $\omega = 2\pi f$, $f = 10^{12} Hz$.

Fig. 2 presents the effect of ω_p on effective mode index. As wave frequency increases, characteristic curves shifted towards higher effective mode index. Moreover, when ω_p increases, the plasma responds more strongly to DSWs, leading to greater degree of wave confinement at the interface. Furthermore, higher ω_p reduce the effective mode index and wave frequency band [34-36].

The imaginary part of propagation constant is called propagation loss. The variation in propagation loss or attenuation, under different ω_p is analyzed in Fig. 3. It can be observed that show that propagation loss increases with frequency. Contrary to Fig. 2, as ω_p increases characteristic curves are shifted towards lower frequency regions. The ability to control the effective mode index and propagation loss can be applied in designing efficient plasmonic waveguides, plasma-based sensors, and THz communication systems.

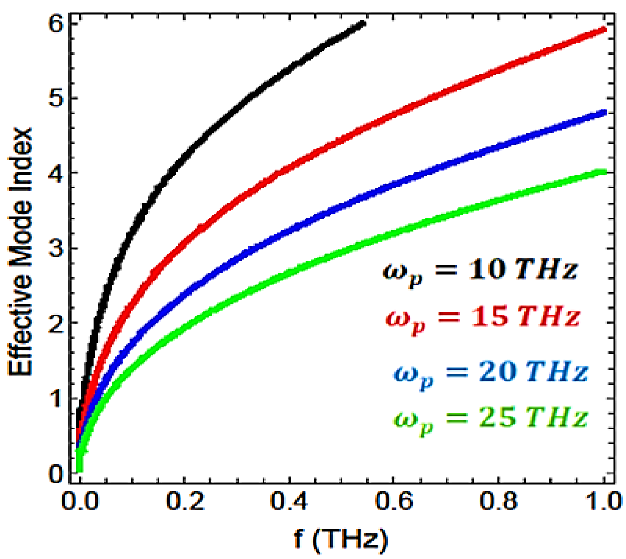

Fig. 2. Influence of ω_p on effective mode index (colour online)

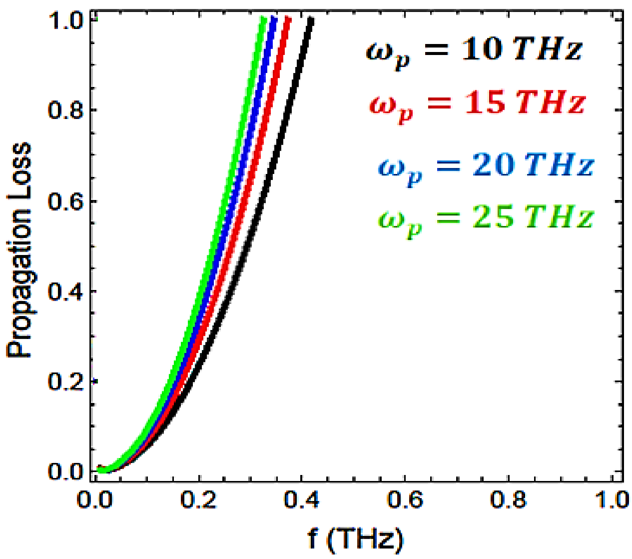

Fig. 3. Influence of ω_p on propagation loss (colour online)

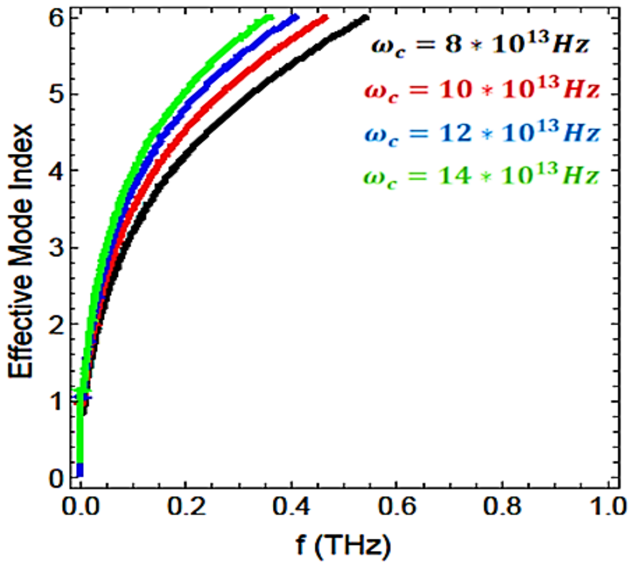

Fig. 4. Influence of ω_c on effective mode index (colour online)

Fig. 4 analyzes the influence of ω_c on effective mode index versus THz wave frequency. Obviously, the effective mode index increases with wave frequency for each value of the cyclotron frequency. It is worthwhile note that at lower wave frequency, characteristic curves exhibit unphysical region that has no practical importance in wave optical community [24, 31]. As ω_c increases effective mode index also increases at faster rate, indicating stronger confinement of the wave near the interface, which could be beneficial for plasmonic sensors and communication systems. Furthermore, higher ω_c shift characteristic curves lower wave frequency regime.

Influence of cyclotron frequency on propagation loss is depicted in Fig. 5. It can be observed that increasing ω_c decrease the propagation loss and characteristic curves shift towards higher wave frequency regions. It is vital to note that, by increasing ω_c frequency band becomes narrower, and slope of characteristic curves decreases. Furthermore, propagation loss increases with wave frequency. The increased propagation loss at higher frequencies indicates greater energy dissipation, which is crucial in practical applications such as in communication systems and sensing.

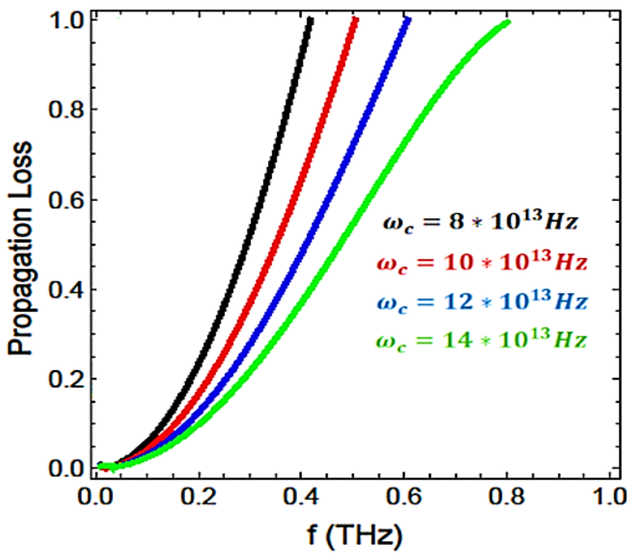

Fig. 5. Influence of ω_c on propagation loss (colour online)

Fig. 6 illustrates the impact of plasma frequency on normalized phase velocity versus THz wave frequency. Normalized phase velocity decreases with increasing wave frequency for all values of ω_p. Furthermore, wave frequency band extends from 0 to 4 THz. Furthermore, highest slope of characteristic curve is achieved at lower value of ω_p. It is vital to note that, wave frequency increases, surface wave interaction with plasma becomes more dispersive, and the characteristic curve flattens, indicating that the phase velocity is less sensitive to changes in plasma frequency at higher frequencies.

Variation in normalized phase velocity under different ω_c is analyzed in Fig. 7. As ω_c increases, normalized phase velocity, and wave frequency band decreases. Furthermore, as the magnetic field strength increases the interaction between the wave and the plasma becomes stronger. This leads to an increase in wave confinement near the plasma surface and a decrease in phase velocity at higher frequencies. It is of peculiar interest to note that, at some higher wave frequency, characteristic curves begin to level off that have no practical importance in the optics community. The former tunability characteristics suggest that DSWs can be engineered by tensorial permittivity parameters of magnetized plasma.

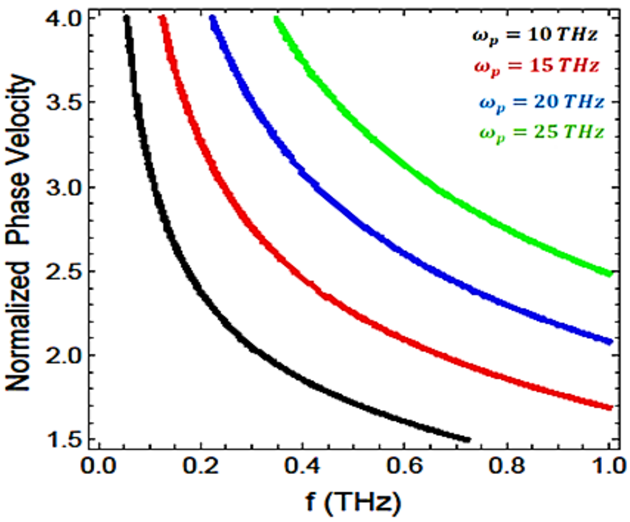

Fig. 6. Influence of ω_p on normalized propagation length (colour online)

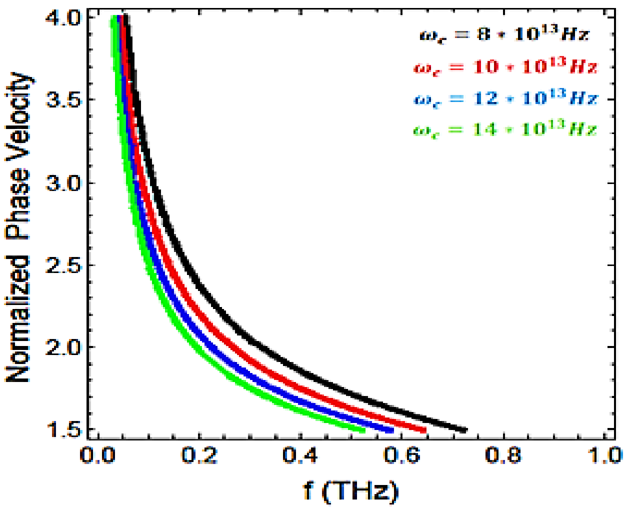

Fig. 7. Influence of ω_c on normalized propagation length (colour online)

Influence of wave frequency on effective mode index versus ω_p is analyzed in Fig. 8. As wave frequency increases, ω_p and effective mode index also increases. Furthermore, as ω_p increases, the effective mode index decreases. This suggests that DSWs propagate faster with increasing ω_p particularly at higher frequencies (1.6 and 1.9 THz). By adjusting wave frequency and plasma frequency, these results can be applied to designing dynamic plasma-based THz waveguides, sensors, imaging systems, communication systems, and modulators.

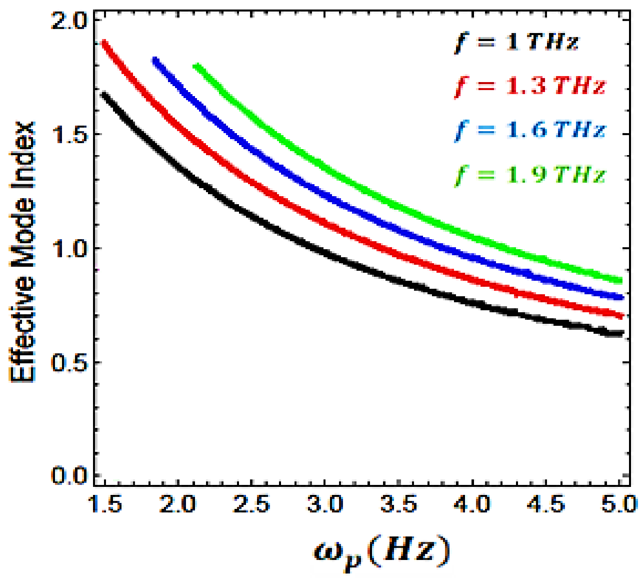

Fig. 8. Influence of wave frequency on effective mode index versus ω_p (colour online)

To verify the conditions for Dyakonov waves, the normalized field profiles in the plasma and free-space medium are analyzed in Figs. 9 and 10, respectively. In both figures, the characteristic curves exhibit exponential decay. Dyakonov waves must satisfy two conditions: (i) the electromagnetic fields decay exponentially away from the interface, and (ii) one of the two dielectric media must be anisotropic [15].

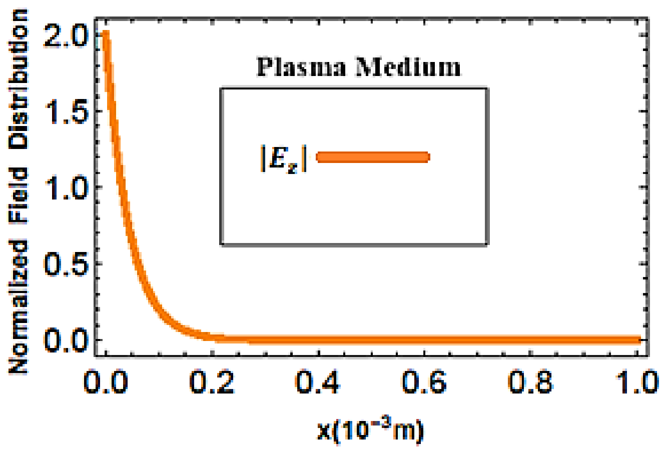

Fig. 9. Normalized field profile for magnetized plasma medium (colour online)

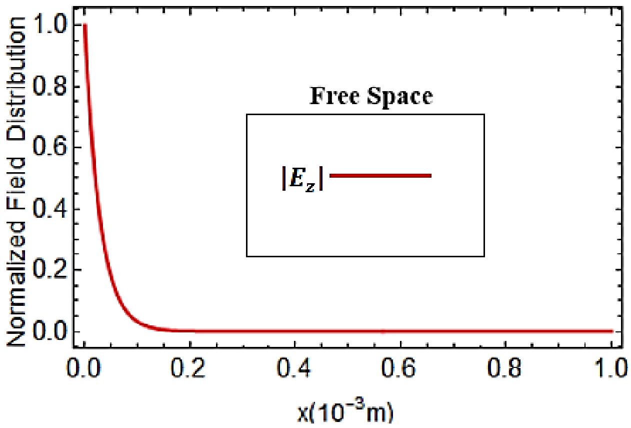

Fig. 10. Normalized field profile for magnetized plasma medium (colour online)

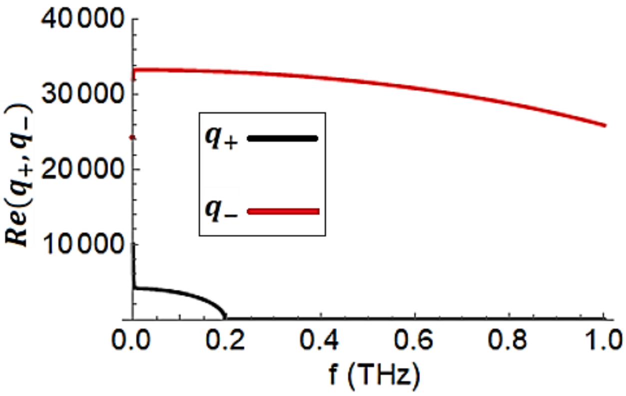

Fig. 11. Real part of decay constant versus wave frequency (colour online)

Fig. 11 presents the decay constants q_+ and q_- versus THz frequency. The larger magnitude of q^- indicates stronger field confinement in plasma medium, whereas the comparatively small q_+ corresponds to weak confinement. The vanishing trend of q_+ near 0.2 THz suggests the cutoff condition beyond which the associated mode becomes weakly bound or radiative.

4. Conclusions

Modeling of DSWs at magnetized plasma–dielectric interface has been performed in THz frequency region and following conclusion:

- The effective mode index increases with wave frequency for varying ω_p and ω_c.
- Effective mode index decreases by increasing ω_p and vice versa for ω_c.
- Propagation loss increases with increasing wave frequency.
- By adjusting tensorial permittivity parameters of magnetized plasma propagation loss can be controlled.
- Normalized phase velocity is also very sensitive to ω_p and ω_c.
- THz wave frequency plays a crucial role in tuning the effective mode index.
- In conclusion, modeling of DSWs at magnetized plasma–dielectric interface in THz frequency region contributes to our comprehension of wave–matter interactions in engineered environments, thereby facilitating advancements in wave propagation, metamaterials, plasma-based sensing systems, and advanced communication systems.

References

[1] L.-C. Crasovan, D. Artigas, D. Mihalache, L. Torner, Optics Letters **30**(22), 3075 (2005).
[2] S. R. Nelatury, J. A. Polo Jr, A. Lakhtakia, Microwave and Optical Technology Letters **50**(9), 2360 (2008).
[3] J. A. Polo Jr, A. Lakhtakia, Laser & Photonics Reviews **5**(2), 234 (2011).
[4] F. Marchevskiĭ, V. Strizhevskiĭ, S. Strizhevskii, Fizika Tverdogo Tela **26**(5), 1501 (1984).
[5] M. Dyakonov, V. Perel, Sov. Phys. JETP **67**, 714 (1988).
[6] A. G. Ardakani, M. Naserpour, C. J. Zapata-Rodríguez, Photonics and Nanostructures-Fundamentals and Applications **20**, 1 (2016).
[7] O. Takayama, D. Artigas, L. Torner, Optics Letters **37**(20), 4311 (2012).
[8] O. Takayama, L. Crasovan, S. Johansen, D. Mihalache, Electromagnetics **28**(3), 126 (2008).
[9] M. Moradi, Scientific Reports **13**(1), 12353 (2023).
[10] M. Zakharchenko, G. Glinskii, Journal of Physics: Conference Series **1851**(1), 012002 (2021).
[11] S. Chen, Z. Shen, W. Wu, J. Opt. Soc. Am. A **31**(9), 1923 (2014).
[12] C. Zhou, T. G. Mackay, A. Lakhtakia, Optik **211**, 164575 (2020).
[13] O. Takayama, L. Crasovan, D. Artigas, L. Torner, Physical Review Letters **102**(4), 043903 (2009).
[14] O. Takayama, P. Dmitriev, E. Shkondin, O. Yermakov, M. Panah, K. Golenitskii, F. Jensen, A. Bogdanov, A. Lavrinenko, Semiconductors **52**(4), 442 (2018).
[15] J. Polo, T. Mackay, A. Lakhtakia, Electromagnetic surface waves: a modern perspective, Newnes, Elsevier Inc. 2013.
[16] M. Umair, A. Gaffar, M. A. S. Alkanhal, Y. Khan, A. H. Alqahtani, Plasmonics **18**(3), 1029 (2023).
[17] K. Miyamoto, Plasma physics for nuclear fusion, Cambridge, Mass., MIT Press, 1980, 625 p. Translation, 1980.
[18] D. R. Nicholson, Introduction to plasma theory, Wiley New York, 1983.
[19] D. G. Swanson, Plasma Waves, CRC Press 2003.
[20] M. Yaqoob, A. Ghaffar, I. Shakir, M. Y. Naz, M. Sarfraz, S. Ahmed, Q. A. Naqvi, Optoelectron. Adv.

Mat. **8**(11-12), 1150 (2014).
[21] M. Moradi, A. Niknam, Physical Review B **98**, 085403 (2018).
[22] M. Moradi, A. R. Niknam, Optics Letters **43**(3), 519 (2018).
[23] M. A. Alkanhal, A. Ghaffar, Journal of the Optical Society of America A **32**(12), 2316 (2015).
[24] R. Ali, B. Zamir, H. Shah, Results in Physics **8**, 243 (2018).
[25] M. Z. Bani-Fwaz, R. Bousbih, R. Khamis, M. S. Soliman, Plasmonics **20**(3), 1523 (2025).
[26] M. Shaban, S. J. Aqool, G. S. Yaseen, I. A. Ali, Plasmonics **20**, 3257 (2024).
[27] M. Shaban, K. H. Salem, R. S. Alnayli, A. Waleed, Plasmonics **20**(6), 3919 (2025).
[28] M. Umair, A. Ghaffar M. A. Alkanhal, Y. Khan, M. U. Shahid, M. A. Ali, Scientific Reports **15**(1), art. no. 14801 (2025).
[29] B. Zamir, R. Ali, Journal of the Korean Physical Society **72**(10), 1166 (2018).
[30] T. Zia, L. Bangfan, Z. F. Khudhair, M. Shaban, Optical and Quantum Electronics **57**(6), 325 (2025).
[31] M. Shaban, R. A. Khamis, M. S. Jabir, H. Majdi, Laiba, N. M. A. HadiaA. Waleed, Optical and Quantum Electronics **56**(9), 1471 (2024).
[32] M. A. Alkanhal, M. Umair, A. Ghaffar, M. Y. Naz, A. H. Alqahtani, Y. Khan, Optik **229**, 166255 (2021).
[33] J. Gong, Journal of Plasma Physics **62**(1), 87 (1999).
[34] M. Arif, M. Umair, A. Ghaffar, M. Z. Yaqoob, Kashf Journal of Multidisciplinary Research **2**(04), 200 (2025).
[35] M. Umair, A. Ghaffar, M. A. S. Alkanhal, M. Y. Naz, Ali H. Alqahtani, Y. Khan, Journal of Electromagnetic Waves and Applications **35**(2), 150 (2021).
[36] M. Umair, A. Ghaffar, M. A. S. Alkanhal, Y. Khan, Ali H. Alqahtani, I. Shakir, Plasmonics **18**(5), 1857 (2023).

APPENDIX:

The EM fields in magnetized plasma medium are as follows:

$$E_{z1} = (A_1 e^{-q_1 x} + A_2 e^{-q_2 x}) e^{-j\beta z} \tag{A}$$

$$H_{z1} = j(A_1 \alpha_1 e^{-q_1 x} + A_2 \alpha_2 e^{-q_2 x})\, e^{-j\beta z} \tag{B}$$

$$E_{x1} = -je^{-j\beta z - x(q_2 - q_1)}(e^{-q_2 x} q_1 (a + c\alpha_1) A_1 + e^{-q_1 x} q_2 (a + c\alpha_2) A_2) \tag{C}$$

$$E_{y1} = e^{-j\beta z - x(q_2 - q_1)}(e^{-q_2 x} q_1 (b - d\alpha_1) A_1 + e^{-q_1 x} q_2 (b - d\alpha_2) A_2) \tag{D}$$

$$H_{x1} = e^{-j\beta z - x(q_2 - q_1)}(-e^{-q_2 x} q_1 (e - a\alpha_1) A_1 - e^{-q_1 x} q_2 (e - a\alpha_2) A_2) \tag{E}$$

$$H_{y1} = je^{-j\beta z - x(q_2 - q_1)}(e^{-q_2 x} q_1 (f_1 + b\alpha_1) A_1 - e^{-q_1 x} q_2 (f_1 + b\alpha_2) A_2) \tag{F}$$

The fields phasor for free space is given below:

$$E_{y2} = A_3\, e^{\gamma x} e^{-j\beta z} \tag{G}$$

$$H_{y2} = A_4\, e^{\gamma x} e^{-j\beta z} \tag{H}$$

$$E_{z2} = A_4 (\tfrac{j\gamma}{\omega \varepsilon_0})\, e^{\gamma x} e^{-j\beta z} \tag{I}$$

$$H_{z2} = A_3 (-\tfrac{j\gamma}{\omega \mu_0})\, e^{\gamma x} e^{-j\beta z} \tag{J}$$

To obtain the characteristics equation, we have applied the boundary conditions at $x = 0$.

$$\hat{x} \times (H_1 - H_2) = 0 \tag{K}$$

$$\hat{x} \times (E_1 - E_2) = 0 \tag{L}$$

$$A = \begin{bmatrix} a_{11} & a_{12} & a_{13} & a_{14} \\ a_{21} & a_{22} & a_{23} & a_{24} \\ a_{31} & a_{32} & a_{33} & a_{34} \\ a_{41} & a_{42} & a_{43} & a_{44} \end{bmatrix} \begin{bmatrix} A_1 \\ A_2 \\ A_3 \\ A_4 \end{bmatrix} = 0 \tag{M}$$

where,

$a_{11} = j\alpha_1,\ a_{12} = j\alpha_2,\ a_{13} = \frac{j\gamma}{\omega\mu_0},\ a_{14} = 0,\ a_{21} = jq_1(f_1 + b\alpha_1),\ a_{22} = jq_2(f_1 + b\alpha_2),\ a_{23} = 0,\ a_{24} = -1,$ $a_{31} = q_1(b - d\alpha_1),\ a_{32} = q_2(b - d\alpha_2),\ a_{33} = -1,\ a_{34} = 0,\ a_{41} = 1,\ a_{42} = 1,\ a_{43} = 0,\ a_{44} = \frac{j\gamma}{\omega\varepsilon_0}.$

The solution of above matrix is given below:

$$\gamma q_2(-b\varepsilon_0\omega + \alpha_2(d\varepsilon_0\omega + (b^2 + df_1)\gamma q_1) - (\mu_0\omega(f_1 + b\alpha_2) + (b^2 + df_1)\gamma q_1)\alpha_1) + \omega(b\gamma\varepsilon_0 q_1 - \varepsilon_0(\mu_0\omega + d\gamma q_1)\alpha_1 + \mu_0\alpha_2(\varepsilon_0\omega + \gamma q_1(f_1 + b\alpha_1))) = 0 \qquad (N)$$

*Corresponding authors: rumair.uaf@gmail.com;
aghaffar16@uaf.edu.pk